The Mean Summer and Fall Circulation of Western Bank on the Scotian Shelf

G.G. Panteleev[†] and B. deYoung[*]
Department of Physics and Physical Oceanography, Memorial University of Newfoundland, St. John's, NF A1B 3X7

and

M. Yaremchuk
International Pacific Research Center, SOEST, University of Hawaii, Honolulu, U.S.A.

[Original manuscript received 6 October 1999; in revised form 25 January 2001]

ABSTRACT *The mean climatological circulation on the central Scotian Shelf was investigated during the summer (August–September) and late fall (November–December) by applying a diagnostic model coupled with a variational approach. Historical Conductivity-Temperature-Depth (CTD) profiles, current meter observations and atmospheric climatological data were applied to the model. The reconstructed fields of temperature, salinity and velocity are dynamically balanced and provide estimates of the circulation features on Western Bank for the summer and fall. The availability of new direct current measurements on and around Western Bank enabled us to define the barotropic velocity field and to produce realistic circulation patterns.*

The primary difference between the summer and fall circulation is the intensification of the surface flow field in the fall. The transport of the Nova Scotia current increases from 0.4 Sv in summer to 0.9 Sv in the fall. At the same time, some qualitative differences were found over Western Bank and in Emerald Basin. Applying the variational assimilation procedure at high resolution (6 km) produced narrow currents (roughly 20–40 km across) in agreement with the structure of the local topography and current meter observations.

RÉSUMÉ *[Traduit par la rédaction] La climatologie de la circulation moyenne sur le centre de la plate-forme Scotian a fait l'object d'une étude au cours de l'été (août/septembre) et tard à l'automne (novembre/décembre) en utilisant un modèle diagnostique couplé avec une approche variationnelle. On a exécuté le modèle avec des profils historiques de Conductivité/Température/Profondeur (CTP), des observations de courantomètres et des données climatiques atmosphériques. Les champs reconstitués de température, de salinité et de vitesse sont équilibrés dynamiquement et fournissent des estimations des caractéristiques de la circulation sur le banc Ouest, pour l'été et l'automne. La disponibilité de nouvelles mesures directes de courants sur le banc Ouest et tout autour nous a permis de définir un champ de vitesse barotrope et de produire des configurations réalistes de la circulation.*

La différence importante entre la circulation de l'été et de l'automne, c'est l'intensification du champ de l'écoulement de surface en automne. Le mouvement du courant de la Nouvelle-Écosse augmente de 0,4 Sv en été à 0,9 Sv à l'automne. En même temps, on a trouvé quelques différences qualitatives sur le banc Ouest et dans le bassin Emerald. L'exécution du système d'assimilation variationnelle à fine résolution (6 km) a produit des courants étroits (plus ou moins de 20 à 40 km de large) en accord avec la structure de la topographie locale et des observations de courantomètres.

1 Introduction

Earlier studies of the circulation of the Scotian Shelf focused on the mean water properties and circulation (McLellan et al., 1953; McLellan, 1954; Smith and Petrie, 1982), while more recent work has focused on the time dependent circulation and the interaction between external forcing, stratification and topography (Smith and Schwing, 1991; Sanderson, 1995; Thompson and Griffin, 1998). Of particular interest here is the work on Western Bank, which has been the subject of many studies over the past ten years. One reason for the ongoing interest in Western Bank is that it is an important spawning ground for many different fish species on the Shelf (Taggart et al., 1996; Reiss et al., 2000) and indeed may be

[†]Also Shirshov Institute of Oceanology, Nakhimovsky Prospect 36, Moscow 117218, Russia.
*Corresponding author's e-mail: bdeyoung@physics.mun.ca

the most productive biological region on the Scotian Shelf. Another reason for the interest in Western Bank is that it is easy to reach, just a few hours by ship from Halifax. It is not really known why this particular bank is so biologically productive (Brander and Hurley, 1992) and whether there is a link to the circulation and water properties over the Bank. This work is a component of a larger program to address the latter question. Our greater understanding of the summer and fall circulation on the Bank underlies our other efforts (Reiss et al., 2000) to relate the circulation to the larval patterns of distribution and productivity.

Western Bank, situated at the edge of the Scotian Shelf (Fig. 1), is just one bank within a system of banks on the Nova Scotian shelf. Its importance is determined by its relatively large spatial extent (120 km long, 60 km across, but covering less than 10% of the total area of the shelf) and its location near the continental slope. As a consequence of its location, at least five water masses can influence water properties on Western Bank. According to Houghton et al. (1978) and McLellan (1954), local water properties are defined by fresh cold surface water outflow from the Gulf of St. Lawrence, subsurface (100–150 m) cold water flowing from Cabot Strait, surface slope water, warm and salt intermediate (100–150 m) slope water and deep (200–300 m) slope water. Geographically, this shelf break region is a key location for the exchange of water between the open ocean and the shelf and the investigation of its circulation is of particular interest for the definition of the mean cross shelf transport (Loder et al., 1997).

Our knowledge of the circulation on the Scotian Shelf has expanded substantially over the past decade (Han et al., 1997; Loder et al., 1997; Sheng and Thompson, 1996; Greenberg et al., 1997). Sheng and Thompson (1996) successfully applied a modified dynamic height model to the shelf. They found good agreement between their model and independent measurements. They concluded that baroclinic effects dominate the circulation pattern on the Shelf. Han et al. (1997) investigated the seasonal, bi-monthly, circulation and pointed out the strong difference in the intensity of summer and winter circulation. Greenberg et al. (1997) applied a finite element model to investigate the spatial and temporal response of the barotropic pressure field to wind forcing. They determined the role of topography in guiding cross-shelf subsurface flow that develops in response to cross-shelf Ekman transport.

Previous studies have determined that the circulation over Western Bank is strongly anti-cyclonic (Sanderson, 1995; Griffin and Thompson, 1997) with typical surface velocities of 10 cm s^{-1}. Previous direct measurement of the current on Western Bank (Thompson and Griffin, 1998) enabled us to estimate the mean spatial correlation scale for the velocity field, which we found to be about 35 km. Surrounding the bank, are several relatively narrow channels (20–40 km across) that play an important role in steering the flow around the bank and are associated with small-scale features of the mean flow.

We limit our attention to Western Bank, thereby allowing us to carry out our analysis at greater resolution than have previous investigators. The application of a variational algorithm allows us to incorporate hydrographic data (temperature and salinity), meteorological data and current data, including data collected in the area during 1997 and 1998. We will average the current meter time-series data to provide estimates of the mean circulation. We are interested in the summer and fall period because of the availability of hydrographic and current data for this period and because of the biological interest (Reiss et al., 2000) in the influence of the summer and fall circulation on the growth and retention of fish larvae around Western Bank.

One persistent difficulty in determining the characteristics of circulation and hydrography on the continental shelf is the irregular distribution of the observations. The analysis of the historical distribution of temperature-salinity data (see Fig. 1b) for this region revealed strong irregularities, particularly just off the shelf. For example observations of density data at ocean depths greater than 300 m decrease dramatically from 14.5 station per 1000 km^2 to 1.2 station per 1000 km^2. Such irregular spacing usually requires interpolation (Gandin, 1963; Bretherton et al., 1976) onto a regular grid and, as a consequence, a preliminary knowledge of the correlation function which, with limited data, can be a source of error (McIntosh, 1990). Here we shall develop a different approach. Taking into account the topographic features in the region and the several open boundaries, we applied a data assimilation technique (Wunsch, 1994; Grotov et al., 1998; Griffin and Thompson, 1996). This technique provides a natural way to infer open boundary conditions by incorporating the available data into an ocean circulation model. The assimilation technique employed is one recently developed and successfully applied to the Southern Ocean (Nechaev et al., 1997; Grotov et al., 1998). The main difference between the technique as applied here and that of Nechaev et al. (1997) and Grotov et al. (1998) lies in the treatment of the temperature and salinity as control variables rather than density. We have also made some modifications to the cost function, which we defined based upon our knowledge of the topography and the data distribution.

The paper is organized as follows. In the next section, the climatological data used for the inversion are presented. In Section 3, we briefly outline the dynamical constraints and the method of data assimilation. A more detailed description of this approach is given by Nechaev et al. (1997). The results of the data assimilation and a simplified sensitivity analysis are presented in Sections 4 and 5. A discussion of the summer and fall circulation features and conclusions complete our presentation.

2 The data

We used four different kinds of data for our analysis: (1) hydrographic data; (2) current meter data; (3) sea surface flux data; and (4) transport data.

a *Hydrographic Data*

We obtained profiles of temperature and salinity from the Bedford Institute of Oceanography (courtesy of K. Drinkwater). We used only combined salinity and temperature vertical pro-

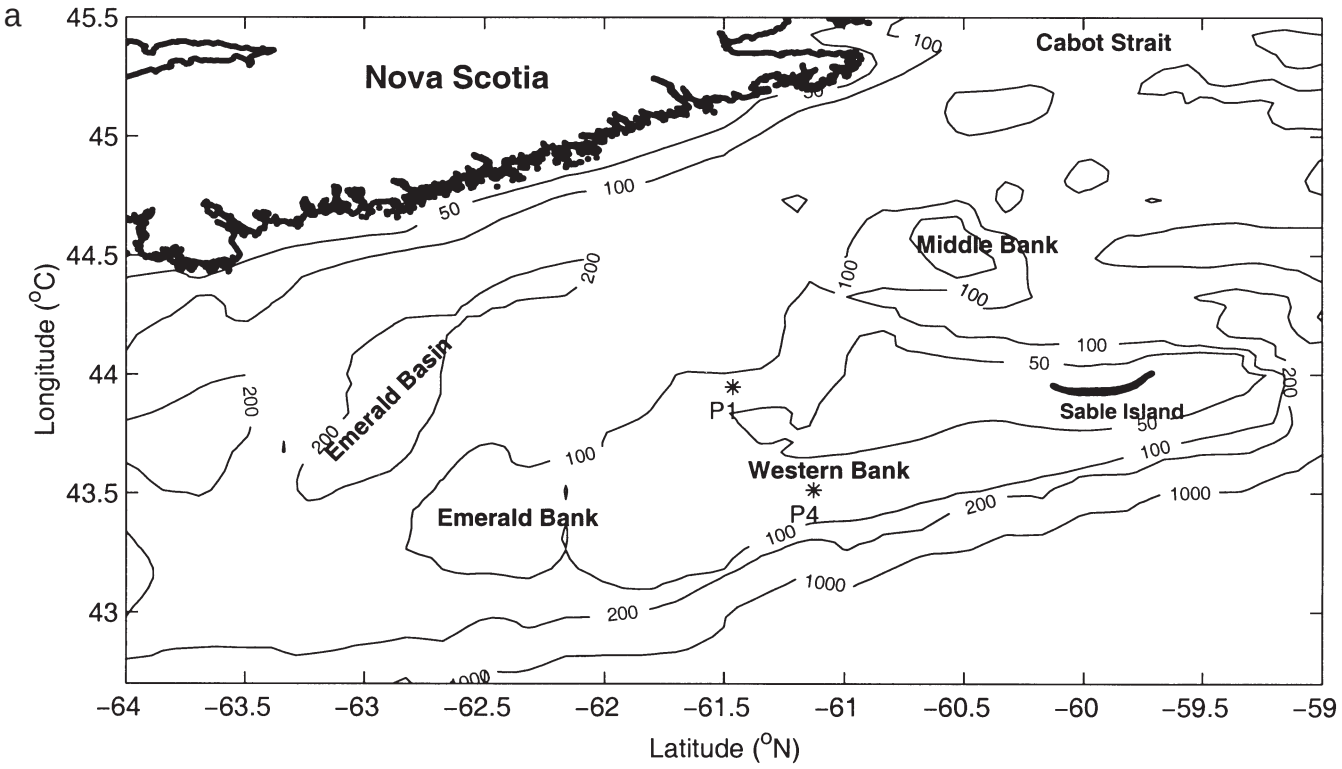

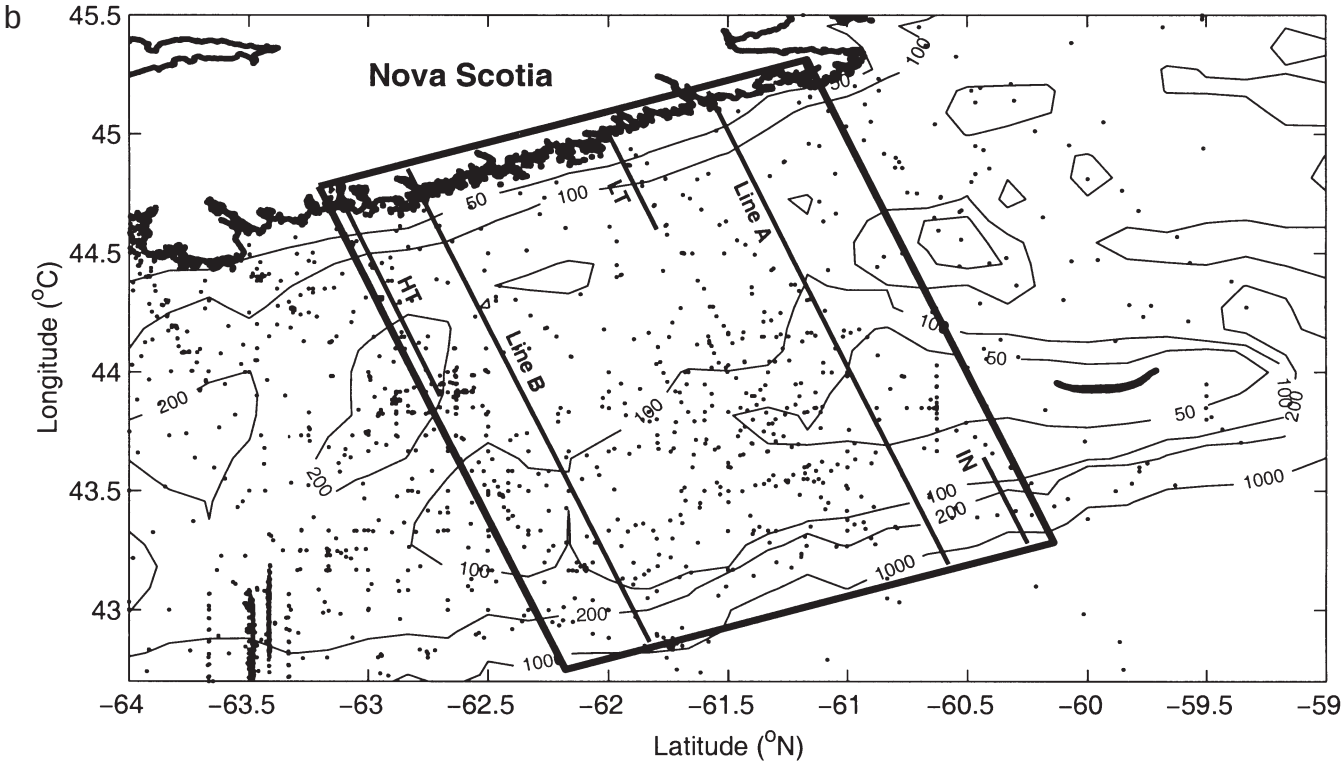

Fig. 1 (a) Map showing the location of Western Bank and primary topographic features of the Scotian Shelf. Water depth is in metres. The locations of the two moorings deployed in 1997 are marked P1 and P4. (b) Study area with the distribution of the assimilated temperature and salinity data (black points). Legend: HT - Halifax transect; LT - Liscomb transects; IN - "inflow" transect trough the along slope current; A - line A; B - line B; EB - Emerald Bank; WB - Western Bank; MB - Middle Bank; Em.B - Emerald basin.

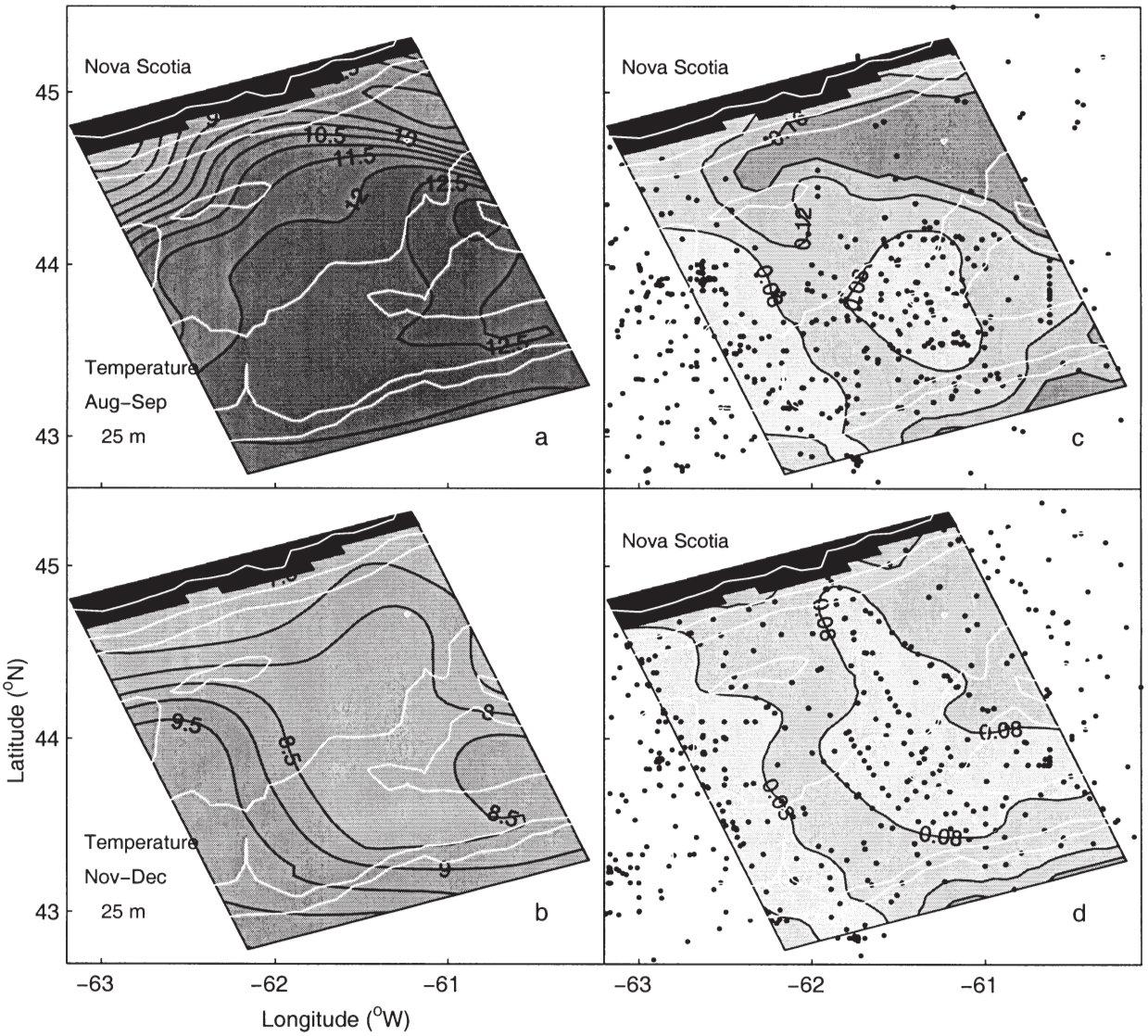

Fig. 2 Initial optimally interpolated temperature field on 25 m for summer (a) and fall (b) periods. (c),(d) are the errors as determined by the variational algorithm.

files where the sampling depth exceeded 20 m. Deep temperature-only casts were removed from the data for two reasons. Firstly, use of temperature data without the corresponding salinity often caused static instability of the water column since interpolated salinity is then needed to compute density. As convective adjustment and its adjoint are strongly nonlinear procedures, the proposed interpolation algorithm is quite computationally demanding. Secondly, as will be shown, salinity provides the major contribution to the stratification and circulation on the Scotian Shelf, suggested earlier by Petrie and Drinkwater (1993).

For the period 1915–1996, we extracted 1657 and 897 profiles, for the summer and fall periods respectively, from the historical data for the region with coordinates 42°–46°N, 59°–64°W. These profiles were combined with the 115 summer and 215 fall profiles that we collected in 1997 and 1998. The hydrographic data were interpolated onto a regular grid by applying a standard optimal interpolation method (Gandin, 1963) with a Gaussian correlation function. The resolution of the horizontal grid was about 5 km. The vertical resolution was 5–10 m near the surface gradually increasing below 150-m depth. We chose a relatively small correlation radius (17 km) since we wanted our variational algorithm to provide dynamical smoothing for the final interpolation. Over the slope we took into account prior knowledge about along-slope anisotropy and gradually increased the along-slope correlation radius up to 27 km in the regions where the depth was 200–1000 m, keeping the cross-slope scale at 17 km. The vertical grid has 25 levels with a maximum depth of 1000 m. The use of such a short correlation scale does generate some gaps in the interpolation scheme and leads to some non-physical features. For example the “optimal” summer temperature distribution on Fig. 2a has a narrow front in the north-eastern part of our region where there are few data, while the fall temperature (Fig. 2b) has an unusually abrupt 8.5°C isotherm in the south-eastern corner.

As mentioned above, the spatial distribution of the data was rather irregular. In regions deeper than 300 m, we had disproportionately fewer measurements (< 1% of the total). During summer, measurements were sparse in the north-eastern part of our region (< 2%). Optimal interpolation errors were calculated and taken into account in formulating temperature and salinity variance dependence upon the spatial coordinates.

b *Current Meter Data*

Estimates of the mean and low-frequency variance for the summer and fall climate velocities were compiled from monthly averaged measurements kindly provided to us from the Bedford Institute of Oceanography (courtesy of D. Gregory). From these data, we extracted and calculated seasonal averages from the observations in the layers between 20–50 m and 50–80 m. Most of the extracted data were initially created from velocity time series more than 10-days' duration, except for 2 records from the summer and 3 from the fall. The computed averages were attributed to levels at 35 m and 65 m respectively. We ignored measurements in the upper layer as they can be influenced by the surface boundary layers. Velocity measurements from deeper levels than (80 m), and observations just outside the model domain, were set aside for the model-data comparison. In total, we found 33 and 36 velocity averages for the summer and fall periods respectively.

c *Surface Fluxes*

Heat and salt surface fluxes were obtained from the monthly climatology compiled by Da Silva et al. (1994). Mean values were about +80 W m^{-2} for the summer and –50 W m^{-2} for the fall, both rather close to those estimated by Isemer and Hasse (1987). Wind stress for the Sable Island region was recalculated following Large and Pond (1982) from bi-monthly averaged surface wind provided by the Meteorological Service of Canada (MSC). The spatial structure of the wind stress was compiled in accordance with the bi-monthly averaged spatial structure of the wind stress generated by Da Silva et al. (1994). For this, we have multiplied Da Silva wind stress by 0.7 to re-scale the stress relative to the observed wind stress on Sable Island.

d *Transport Estimates*

For the fall period, we used estimates of 1.1 ± 0.3 Sv and 0.7 ± 0.2 Sv for the transport through the Halifax and Liscomb lines (Fig. 1) respectively (Anderson and Smith, 1989). Taking into account the model results of Han et al. (1997) for the summer season, we estimated the Halifax line transport to be 0.3 ± 0.15 Sv. Due to the limited amount of temperature and salinity data in the open ocean regions and, as a consequence of the strong smoothing in that part of our domain, we specify a transport of 0.8 Sv through the transect in the south-east corner of the domain. This transport estimate is based both on the available velocity measurements from the outer continental slope and on the results of previous investigators (Han et al., 1997; Sheng and Thompson, 1996). The variance for this transport was set at 0.4 Sv, so the final transport could vary significantly without much influence on the minimized cost function. The net transport through the open boundaries was set to zero.

We did not use satellite altimetry data (Han et al., 1997) because of their relatively coarse resolution and because of the difficulty with tidal aliasing. We did, however, include dynamic height estimates calculated by a modified Helland-Hansen approach (Sheng and Thompson, 1996). This method can be applied if the bottom density does not vary along isobaths, a condition that is met on the Scotian Shelf (Sheng and Thompson, 1996). The dynamic height relative to 500 m was interpolated onto the regular grid in the same way as temperature and salinity were. The 500-m reference level, also selected by Sheng and Thompson (1996), was chosen to provide the best agreement between the calculated and measured velocities in the offshore region. Although this approach produces quite reasonable results (cf. Sheng and Thompson, 1996), the assumption of a single fixed reference level is rather simplistic. In order to limit the constraint of this assumption, we specify a mean variance for the dynamic height at about 60% of its spatial variability. In the estimates of dynamic height variance, we took into account probable errors in the definition of the dynamic height in shallow (<30 m) and deep (>200 m) regions and in areas with a strong gradient in bottom topography.

3 Interpolation method

We apply a variational interpolation algorithm to determine the steady state density and wind driven circulation of the Scotian Shelf following Nechaev et al. (1997) and Grotov et al. (1998). The model underlying the scheme is based upon standard formulations for the steady-state dynamical equations that include the effects of diffusivity of temperature, salinity and momentum and also account for the processes of vertical convective adjustment. The equations are:

$$\rho - \Re(\theta, S, p) = 0 \tag{1}$$

$$p_z + g\rho = 0 \tag{2}$$

$$f(\mathbf{k} \times \mathbf{u}) + \frac{1}{\rho_0}\nabla p - D_m \Delta \mathbf{u} - (K_m \mathbf{u}_z)_z = 0 \tag{3}$$

$$\nabla \cdot \mathbf{u} + w_z = 0 \tag{4}$$

$$\nabla \cdot (\mathbf{u}\theta) + (w\theta)_{\mathbf{z}} - (K_\theta \theta_z)_z - D_\theta \Delta\theta - \hat{\Pi}_\theta \theta = F^e_\theta \tag{5}$$

$$\nabla \cdot (\mathbf{u}S) + (wS)_{\mathbf{z}} - (K_S S_z)_z - D_S \Delta S - \hat{\Pi}_S S = F^e_S \tag{6}$$

where $\mathbf{u}$ is the horizontal velocity vector, w is the vertical velocity, D_m, D_θ, D_S, K_m, K_θ and K_S are the horizontal and vertical diffusion coefficients of momentum, potential temperature θ and salinity S respectively; f is the Coriolis parameter; ∇ is the horizontal gradient operator; Δ is the Laplacian operator; g is the acceleration due to gravity; $\mathbf{k}$ is the vertical unit vector; and ρ_0 is a mean density. $\Re$ simply represents the equation of state for seawater rewritten from the UNESCO

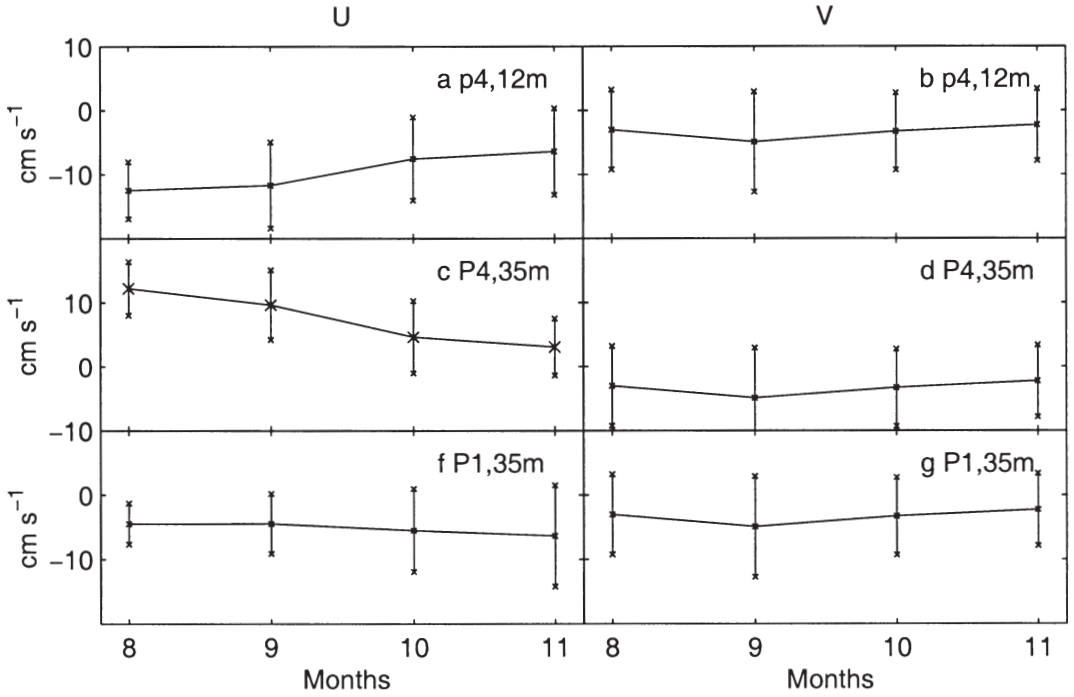

Fig. 3 Monthly averaged long-shore (U) and across-shore (V) velocity components observed at the southern (P4) and northern (P1) flank of the Western Bank during 1997. The length of the lines shows the standard deviation.

(1981) formulation in terms of θ, S and p by Ishizaki (1994). The fields of F^e_θ, F^e_S account for poorly known errors in parametrization of the mixing processes and for temperature and salinity evolution at timescales larger than some prescribed period T^*. The operator $\hat{\Pi}$ describes the vertical convection processes (see the appendix in Grotov et al. (1998)).

Boundary conditions are applied at the surface, the bottom and along the lateral boundaries. At the ocean surface, $z = 0$, we impose the rigid-lid condition (Gill, 1982) and specify the fluxes of momentum, potential temperature and salinity:

$$w = 0$$

$$p - \rho g\zeta = 0;$$

$$K_m \mathbf{u}_z - \boldsymbol{\tau} = 0;$$

$$K_\theta \theta_z - B_\theta = 0;$$

$$K_S S_z - B_S = 0.$$

Here ζ, $\boldsymbol{\tau}$, B_θ and B_S are surface elevation, wind stress and surface heat and salt fluxes.

At the ocean bottom the normal flow, the potential temperature and the salinity fluxes are set to zero:

$$(D_\theta \nabla\theta + \mathbf{k} K_\theta \theta_z) \cdot \mathbf{n} = 0;$$

$$(D_S \nabla S + \mathbf{k} K_S S_z) \cdot \mathbf{n} = 0;$$

$$\mathbf{u} \cdot \nabla H - w - F^w = 0$$

where $\mathbf{n}$ is a normal to the ocean bottom vector. Note, that the last condition is not satisfied exactly. The error level F^w has the order of magnitude of the uncertainty of the Ekman pumping rate into the bottom boundary layer.

At the rigid lateral boundaries, the momentum and tracer fluxes are set to zero. Finally, at the open boundaries, we neglect the diffusive fluxes for momentum, setting the velocities to be purely geostrophic and control the values of θ and S, determining them from the data through the inversion algorithm.

This model is valid for the large-scale, quasi-stationary circulation on the Scotian shelf assuming that the tidal currents do not strongly influence the circulation at timescales of 1–2 months. It is also necessary to assume that we can neglect the advection terms in the momentum equations. Han et al. (1997) conclude that baroclinic circulation is dominant over the Scotian Shelf. For the transport through the Halifax line, Han et al. (1997) estimated that M_2 tidal rectification is 1–2% of the total transport. Furthermore, we expect that our assimilation of observed currents will partly compensate for explicitly ignoring the tides. Typically, for the outer Scotian Shelf, the spatial (50 km) and velocity (10 cm s^{-1}) scales define a Rossby number of about $Ro = 0.02$, so that the influence of the nonlinear terms in the momentum equation should be weak.

Figure 3 shows monthly average long-shore (U) and across-shore (V) velocity components observed on the southern (P4) and northern (P1) flanks of Western Bank during the summer and fall 1997. The monthly-mean currents during these two seasons are nearly time-invariant in the upper layer (Figs 3a,b).

The largest changes in the mean values occurred during October. During the August–September and November–December periods the mean currents remained practically unchanged. We estimate that the variance of the monthly averaged values is related to spreading topographic waves with periods of 7 and 15 days on the flanks of Western Bank. The time-invariant of the monthly-mean observed currents suggests that the seasonal, quasi-stationary circulation that we determine should be physically meaningful.

The inversion algorithm is formulated in terms of the Gaussian probability distribution defined on the data space whose constituents are treated as stochastic δ-correlated functions with unknown means (Thacker, 1989). All the different types of data can be defined within the framework of the dynamical equations (1–6) in terms of the control fields θ, S, ζ, $\boldsymbol{\tau}$, and $B_{\theta,S}$.

Our goal is to find the optimal set that minimizes the following argument of the Gaussian exponent:

$$
\begin{aligned}
\mathcal{J} = & \int_{\Omega} \{W_\theta(\theta-\theta^*)^2 + W_S(S-S^*)^2\} d\Omega \\
& + \int_{z=0} \{W_\theta^B(B_\theta - B_\theta^*)^2 + W_S^B(B_S - B_S^*)^2 + W_\zeta(\zeta-\zeta^*)^2 \\
& + W_\tau(\boldsymbol{\tau}-\boldsymbol{\tau}^*)^2\} d\omega + \sum_{data} \mathbf{W_u}(\mathbf{u}-\mathbf{u}^*)^2 \\
& + \sum_{\alpha=1}^{4} W_\alpha [\int_{L_\alpha} (\mathbf{u}\cdot d\mathbf{n}_\alpha) - F_\alpha^*]^2 + \int_{\Omega} \{W_S^s(\Delta S)^2 + W_\theta^s(\Delta\theta)^2\} d\Omega \\
& + \int_{z=0} \{W_{B_\theta}^s(\Delta B_\theta)^2 + W_{B_S}^s(\Delta B_S)^2 + W_\zeta^s(\Delta\zeta)^2 + W_\tau^s(\Delta\boldsymbol{\tau})^2 \\
& + W_\psi^s(\Delta \int_{-H}^{0} \mathbf{u} dz)^2\} d\omega + \int_{\Omega} \{W_\theta^t(F_\theta^e)^2 + W_S^t(F_S^e)^2\} d\Omega \\
& + W_w \int_{z=-H} (F^w)^2 d\omega.
\end{aligned}
$$

Here Ω is the domain occupied by the computational grid, $\int_{\Omega} d\Omega$, $\int_{z=0} d\omega$, $\int_{z=-H} d\omega$ are integrals over the domain Ω, surfaces $z = 0$ and $z = -H$. $\int_{L_\alpha} (\mathbf{u}\cdot d\mathbf{n}_\alpha)$ is a transport over the transects discussed in the data section. The unit vector $\mathbf{n}_\alpha$ is normal to the transects. F_α^* is the estimate of the transport through these transects. θ^*, S^*, B_θ^*, B_S^*, ζ^*, $\boldsymbol{\tau}^*$ and $\mathbf{u}^*$ are the data for temperature, salinity, surface heat flux, surface salt flux, surface elevation, wind stress and velocity respectively. The weight functions W_θ, W_θ^s, W_θ^t, W_S, W_S^s, W_S^t, W_w, W_ζ, W_ζ^s, W_τ, W_τ^s, W_B, W_B^s, W_ψ and W_α infer additional information on the variability of the corresponding fields. According to the variational algorithm formulation (Thacker, 1989), the functions W^{-1} represent the covariance functions of the corresponding physical values. In the present work, their structure was taken to be diagonal (i.e., a zero cross correlation in space) with diagonal elements depending on space coordinates.

Typical values of $W_{\theta,S}^{-1/2}$ do not exceed 20% of the local spatial variability of the corresponding θ or S data. As an example, in Figs 2 c,d we plot the spatial distribution of $W_\theta^{-1/2}$ normalized by the rms horizontal variability of the potential temperature at 25 m. Assumptions about the smoothness of the temperature and salinity fields take into account the sharper horizontal gradients of these fields observed near the coastline and the banks. Diagonal elements of $W_{\theta,S}^s$ fade near the coast and banks by an order of magnitude, allowing for less smoothness in these regions. The error terms $F_{\theta,S}^e$ are due to treatment of the transport equations in the "weak" form, and can be interpreted as a "degree of unsteadiness" of the solution. Its optimal magnitude depends upon the weight functions $W_{\theta,S}^t$ whose elements were chosen to be inversely proportional to the horizontal variances of the temperature and salinity divided by the timescale T^* that is, 2 months. The variance in the mass exchange with the bottom boundary layer $W_w^{-1/2}$ was specified as a typical Ekman pumping rate. Since shelf regions are typically characterized by strong vertical mixing, we specified a relatively large "acceptable" level of the misfit in the bottom boundary condition with the vertical velocity, about 100 m yr^{-1} defined by estimates of relative vorticity approximately 1×10^{-6} s^{-1} and vertical diffusion 5.0 $\times 10^{-4}$ m^2 s^{-1}.The diagonal elements of W_ζ, W_ζ^s, and W_ψ^s were chosen to be inversely proportional to bottom relief gradients that are important for regulating circulation around the topography:

$$
W_\varphi = \left\{ [10^{-6} + (\nabla H)^2] \int_S (\varphi^* - \overline{\varphi}^*)^2 dS \right\}^{-1}
$$

$$
\varphi^* = \{\zeta^*, \Delta\zeta^*, \Delta\mathbf{U}\} \qquad \mathbf{U} = \int_{-H}^{0} \mathbf{u} dz.
$$

Here, an overbar denotes the average over the sea surface, and $\mathbf{U}$ is the net transport vector of the first-guess state. The variances of atmospheric forcing fields are assumed to be spatially homogeneous, so W_τ, W_τ^s, W_B and W_B^s are assumed to be inversely proportional to the horizontal variances of the corresponding data fields.

Variance estimates of the net transports across Halifax and Liscomb lines during the fall period (Fig. 1b) were estimated as $(W_\alpha)^{-1/2}$ = (0.3, 0.2) Sv. The transport and its variance were calculated by Anderson and Smith (1989) from observed current data. The constrained minimization of $\mathcal{J}$ was performed using a version of a quasi-Newton descent algorithm proposed by Gilbert and Lemarechal (1989). A first-guess state was computed using the control variables specified by the data. Taking into account the nonlinearity of the problem, we minimized $\mathcal{J}$ as outlined in Grotov et al. (1998), gradually increasing the number of control variables starting with the surface elevation ζ and moving up to the full control vector

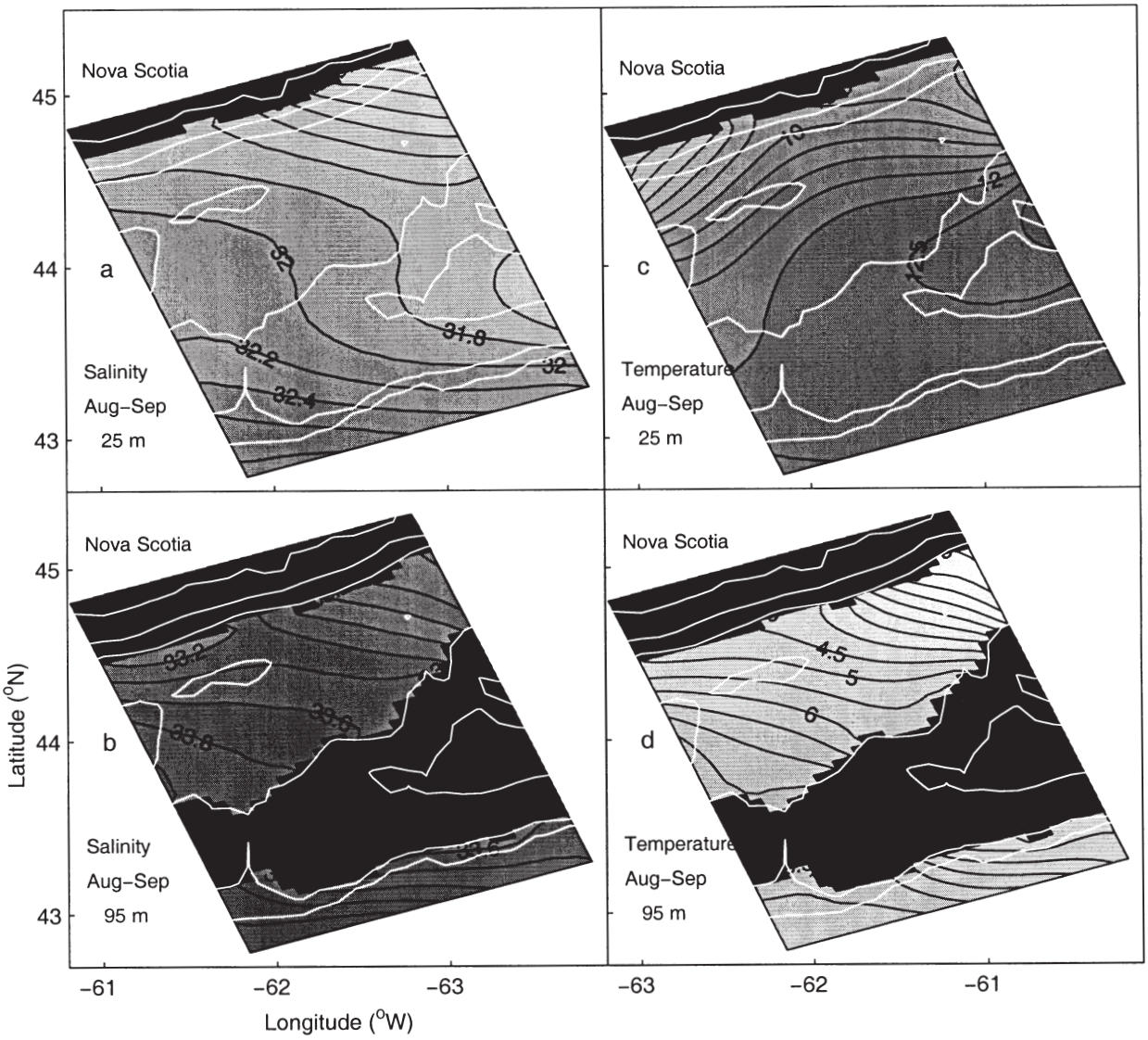

Fig. 4 Optimized salinity (a,b) and temperature (c,d) fields at 25 and 95 m for the summer period.

$\{\theta, S, \zeta, \tau, B_\theta, B_S\}$ whose dimension (the number of grid points occupied by the control fields) was 31,046.

The careful choice of the model error statistics, based on physical considerations and previous experience, enabled us to reduce the cost function by more than fifty times relative to the first-guess state. Since the cost function is related to the Gaussian probability distribution, this reduction can be interpreted as a considerable increase in probability after the introduction of the dynamical constraints, thereby improving the agreement between the model and data.

4 Steady state circulation

a *Hydrographic Fields*

To begin our analysis, we briefly highlight the major hydrographic features of the assimilated temperature and salinity fields. Figures 4 and 5 show the model simulated horizontal temperature and salinity distribution in the upper (25 m) and lower (95 m) layers for the summer and fall respectively. Comparison with the initial temperature distribution at 25 m, obtained by optimal interpolation (Figs 2a,b), shows which modelled fields are smoother and do not have the non-physical features noted above. Increased smoothness is a natural consequence of any interpolation algorithm, however, our algorithm does so through the application of dynamically consistent constraints. Not surprisingly, the modelled temperature and salinity fields retain the principal features of the optimally interpolated data.

The main feature of these distributions is a gradual decrease in temperature and salinity towards the north-east although the subsurface temperature does have some low values near the coast (Figs 4c,5c). According to Houghton et al.

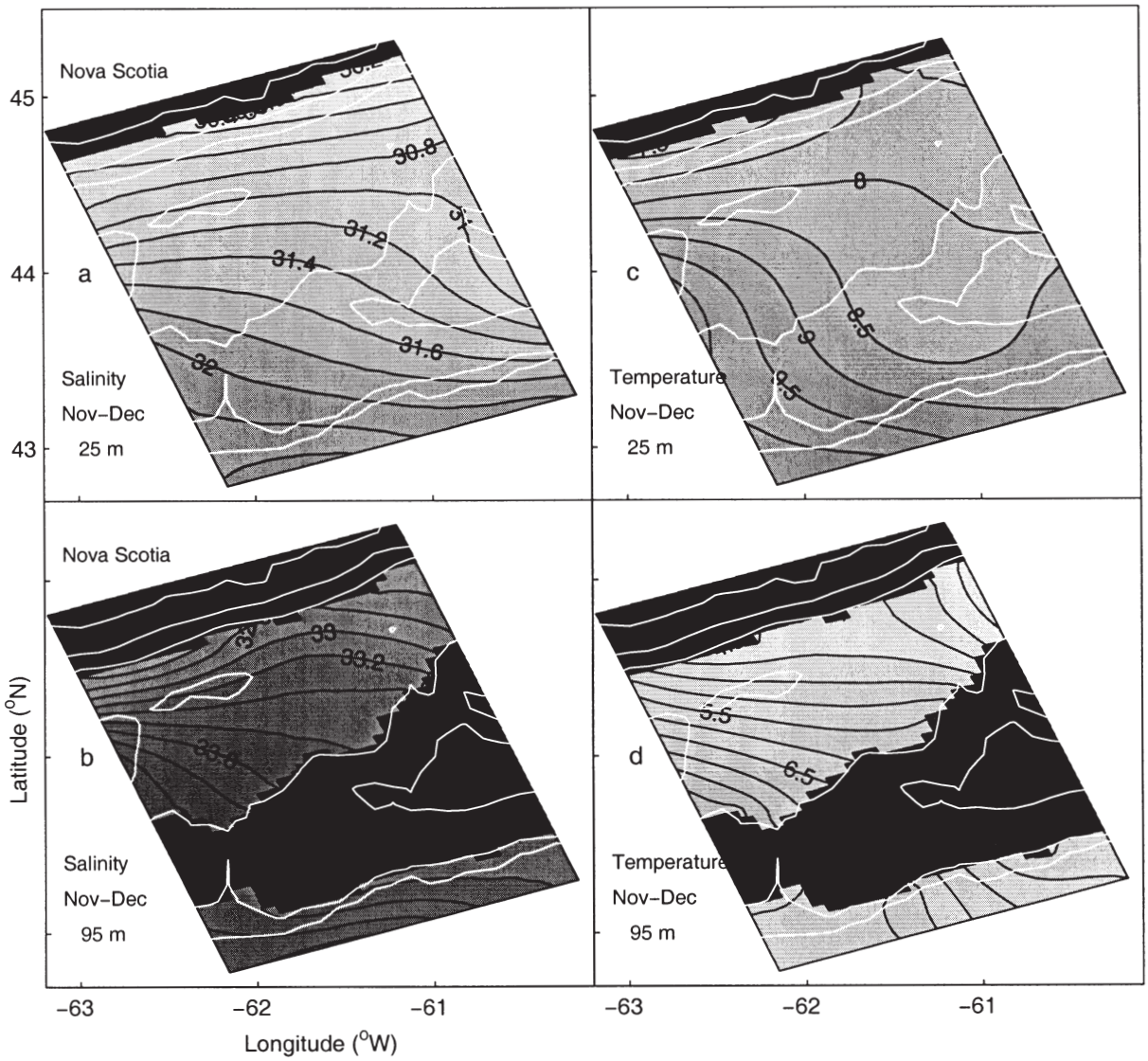

Fig. 5 Optimized salinity (a,b) and temperature (c,d) fields at 25 and 95 m for the fall period.

(1978), this structure is a result of cold surface and subsurface waters penetrating from the Cabot Strait into the north-eastern part of our region and the inflow of warm and salty slope water over Western and Emerald Banks into the Emerald Basin (*cf.* Fig. 1a). The cold water near the coast is connected with the westward movement of subsurface cold water and gradual upwelling near the coastline. In the upper and lower layers, horizontal salinity and temperature variability have values of 2.5 PSU and 5°C. Salinity has a dominant influence on the circulation over most of this region. To illustrate this, we calculated the hypothetical winter circulation assuming isothermal and isohaline water properties and applying the model methodology outlined above. The isothermal circulation is in good agreement (Fig. 6a) with the velocity observations, while circulation defined by temperature alone, the isohaline case (Fig. 6b), is noisy, and does not demonstrate good agreement with the velocity observations. The noise is a consequence of conflict between the velocity defined by temperature alone and the other data (sea surface height (SSH), current and transport through the sections) applied in the interpolation algorithm. Because of this inconsistency between data, we do not draw any quantitative conclusions about the role of temperature and salinity in determining the circulation (Figs 6a,b). We can state qualitatively, however, that on its own the horizontal structure of the temperature tends to generate circulation opposed to the observed mean flow, an effect that is most pronounced in Emerald Basin (Fig. 6b).

The circulation for the isohaline case (Fig. 6b) near the coastline and along Western Bank does coincide with the observed velocity and the modelled velocity field shown below. We conclude that temperature does influence the den-

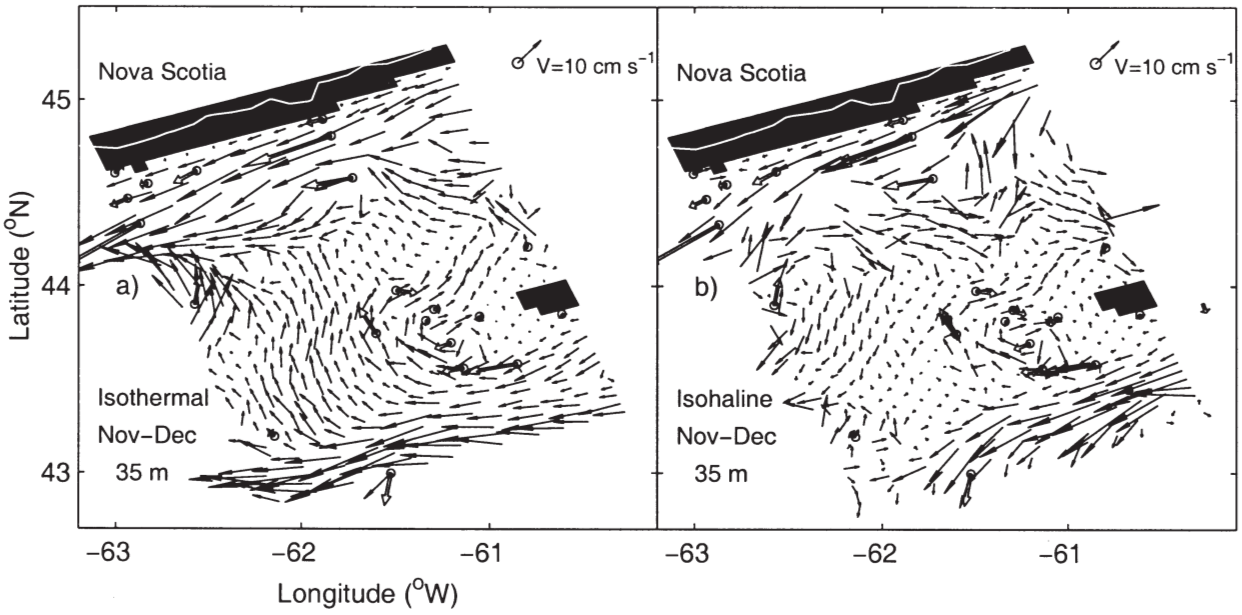

Fig. 6 Hypothetical velocity field on 35 m calculated by proposed algorithm in suggestion of isothermal (a) and isohaline (b) water properties in the investigated region in winter.

sity field near the coastline in the upwelling regions (Figs 4c and 5c) (cf. Petrie and Smith, 1977) and over the shallow banks. Strong vertical mixing that takes place over the banks often leads to strong horizontal temperature gradients between the vertically well-mixed regions on the banks and the less well-mixed, more stratified, regions off the bank (see the 25-m level in Fig. 4c).

Both temperature and salinity distributions on the Scotian Shelf reveal strong seasonal differences near the coast. In summer, the regions with strong across-shelf gradient are in the north-eastern (for salinity Fig. 4a) and northern (for temperature Fig. 4c) parts of our region. In fall, spatial subsurface temperature gradients are more uniform with maxima in the north-western part of our region and between Western and Emerald Banks (Fig. 5). The fall changes are likely due to an increase of estuarine water along the coast and freshening of subsurface water (Figs 4a, 5a). Strong north-west winds which develop during the fall will assist this process by the offshore transport of water in the Ekman layer.

The strong across-shelf gradient in the salinity distribution (Figs 7a,b,e,f) along lines A and B reveals the Nova Scotia Current and a strong along-shelf current along the continental slope. For the Nova Scotia Current this gradient is about 1.5–2 times greater in fall then in summer, thereby suggesting an increase in the fall transport, since the salinity is the primary factor in determining the circulation.

During both the summer and fall, the vertical gradient of salinity is much weaker than for temperature, which can be explained by strong surface heat fluxes (Umoh and Thompson, 1994) in the Nova Scotian region. While salinity increases monotonically with depth, the temperature distribution reveals a strong 3-layered structure with the presence of a cold intermediate layer. According to Umoh and Thompson (1994), the increased depth and lower temperature of this layer during the summer (Figs 7c,d,g,h) is a consequence of the spreading of cold subsurface water from Cabot Strait and seasonal heat fluxes at the surface and mixing with underlying layers. During both seasons, layers deeper than 150 m are occupied by warm (8°C) and salty (> 34 PSU) deep slope water (Houghton et al., 1978).

In summer there is a strong thermocline present over most of the shelf, with a mixed layer that is 20–25 m deep, even over Western Bank. In the fall, strong vertical mixing processes generate uniform, vertical temperature and salinity distribution on Western Bank (Fig. 8) with a mixed layer over the shelf that can reach a depth of 60 m. As an illustration, Fig. 8 shows the observed temperature during the summer and fall of 1998 over the crest of Western Bank.

Naturally the differences between the seasons is greater in the upper layer because of the substantial seasonal shift in atmospheric forcing (Umoh and Thompson, 1994). There is also a stronger horizontal temperature gradient over the western flank of Western Bank in the fall (Fig. 5c) than in summer.

b *Velocity Field and Transports*

Our model treats the temperature/salinity transport equations as "weak" constraints. We define a residual term ($F^e_{\theta,S}$) normalized by the corresponding temperature and salinity variance as a degree of unsteadiness since they are inversely proportional to the timescale T^* of the residual rate of change of the temperature and salinity fields. When so defined, the degree of unsteadiness has typical values of 1.5–2 months reaching a maximum in the 300–1000-m layer. This number corresponds to the temporal scale of the mean seasonal circulation.

Optimized fields of SSH and the total transport function (Fig. 9) demonstrate the main features and seasonal differences of the circulation in our region. In general, these fea-

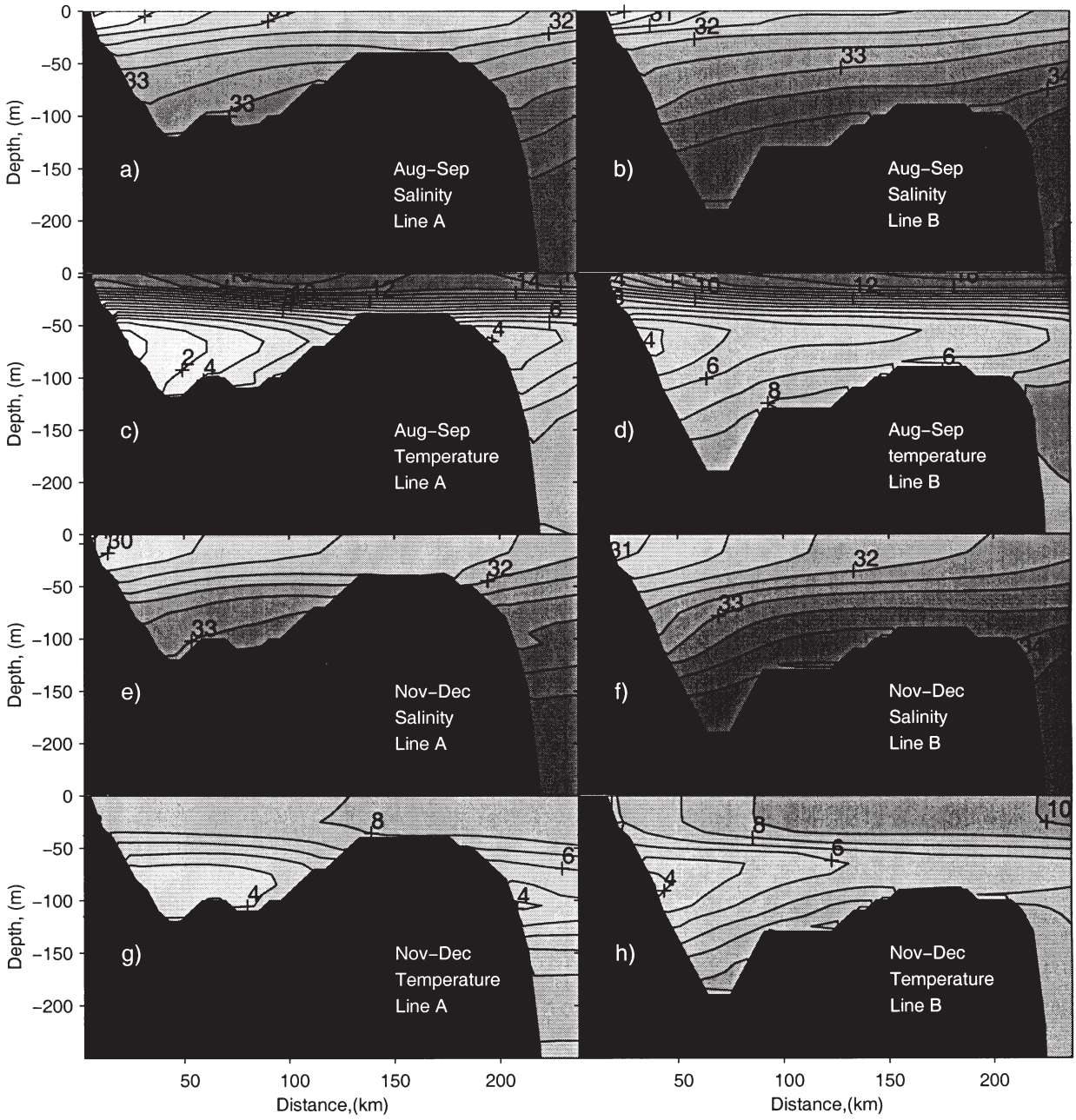

Fig. 7 Optimized temperature and salinity fields at lines A and B shown in Fig. 1 for the summer (a,b,c,d) and fall (e,f,g,h) periods.

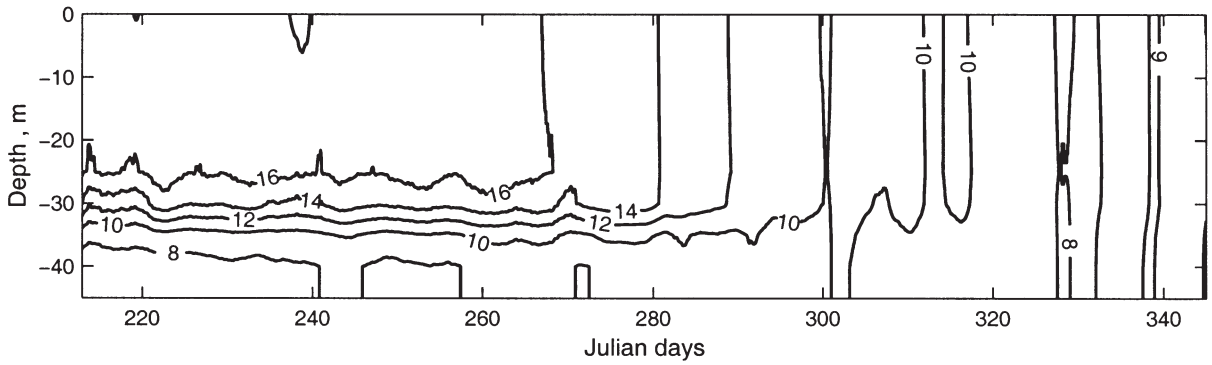

Fig. 8 Typical time dependence for the vertical temperature distribution in the Western Bank region. These data are for 1998 from the crest of the Bank.

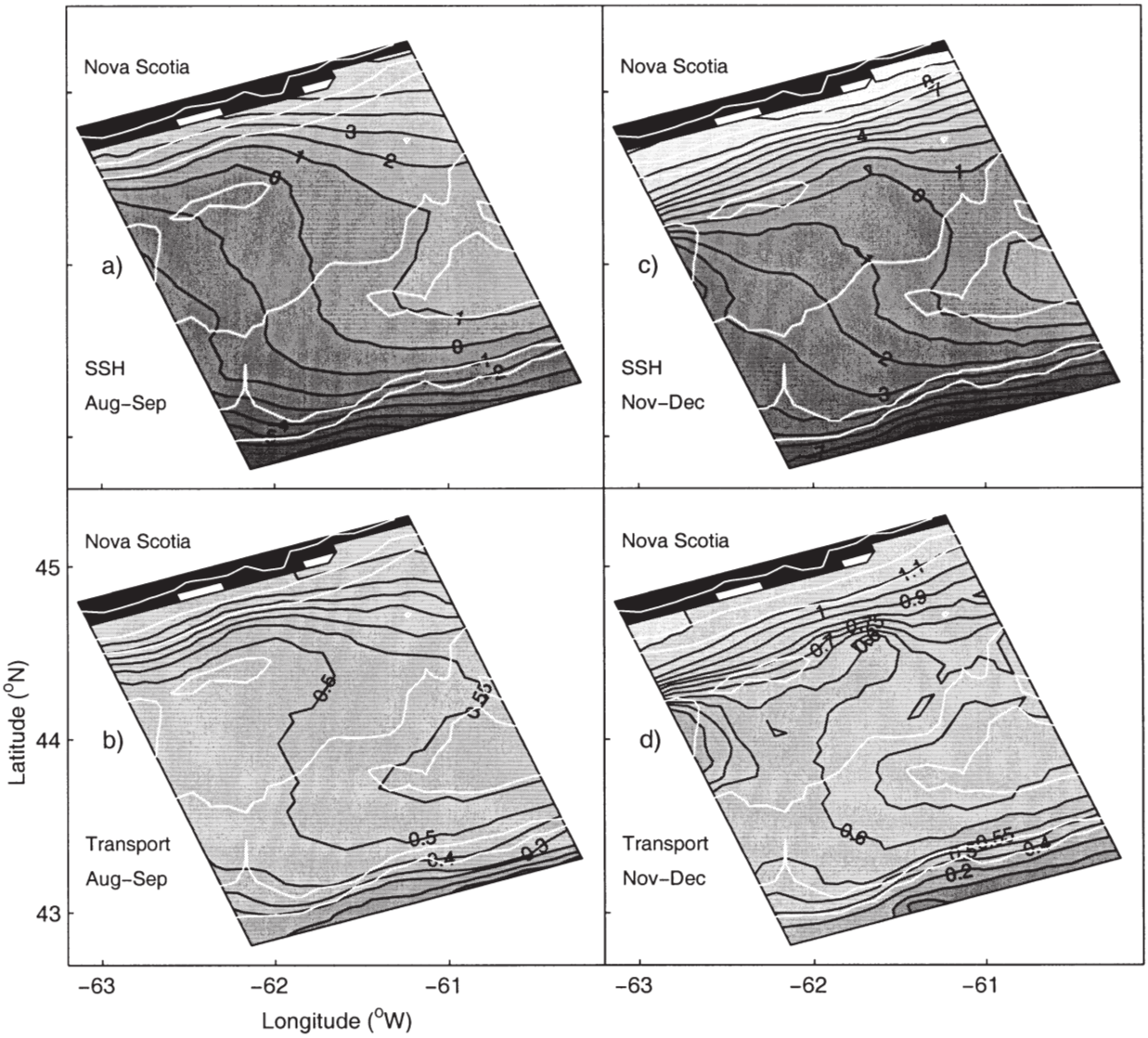

Fig. 9 Sea surface elevation (cm) (a,b) and net mass transport (Sv) (b,d) of the optimal state for the summer and fall periods.

tures correspond to the results of previous investigators (Han et al., 1997; Sheng and Thompson, 1996), although there are some differences. The dominant current on the inner shelf is the Nova Scotia Current (Smith and Schwing, 1991). In the vicinity of the Halifax line, this current has a transport of 0.35 Sv in summer and about 0.9 Sv in the fall. At the same time, the seasonal SSH distributions (Figs 9a and 9c) show some substantial spatial changes in the Nova Scotia Current between summer and fall. In the fall, the distribution is not only twice as broad as in summer but its centre moves about 20 km away from the coast, leaving the nearshore region with a weaker and more diffuse circulation.

In the fall, the transport of the Nova Scotia Current near the Halifax line is formed by flow over the shelf out of the Gulf of St. Lawrence (Fig. 9d), about 0.6 Sv, and by inflow through the Western and Emerald Banks, 0.1 Sv, and the relatively intensive cyclonic circulation in the west part of Emerald Basin, 0.2 Sv. In summer this cyclonic circulation in the Emerald Basin becomes much weaker while the two other currents are, respectively, 0.25 and 0.1 Sv.

Our estimate of the fall transport of the Nova Scotia Current is in good agreement with the lower boundary estimate of Anderson and Smith (1989). Note that here we are assimilating a transport through the Halifax line of 1.1 ± 0.3 Sv. The complicated distribution of the total transport function on the northern flank of the Western Bank during the fall reflects current flowing through the channel between Middle and Western Banks. We speculate that continuation of this current creates a local eastward transport on the northern flank of the Western Bank.

Another clearly identified current runs along the continental slope with a transport of 0.6 Sv and 0.8 Sv in summer and fall respectively. Near the outer edge of the channel (61.5°W and 43°N), between Western and Emerald Banks, the current deflects offshore in agreement with the cyclonic slope gyre described by Csanady and Hamilton (1988). This current can

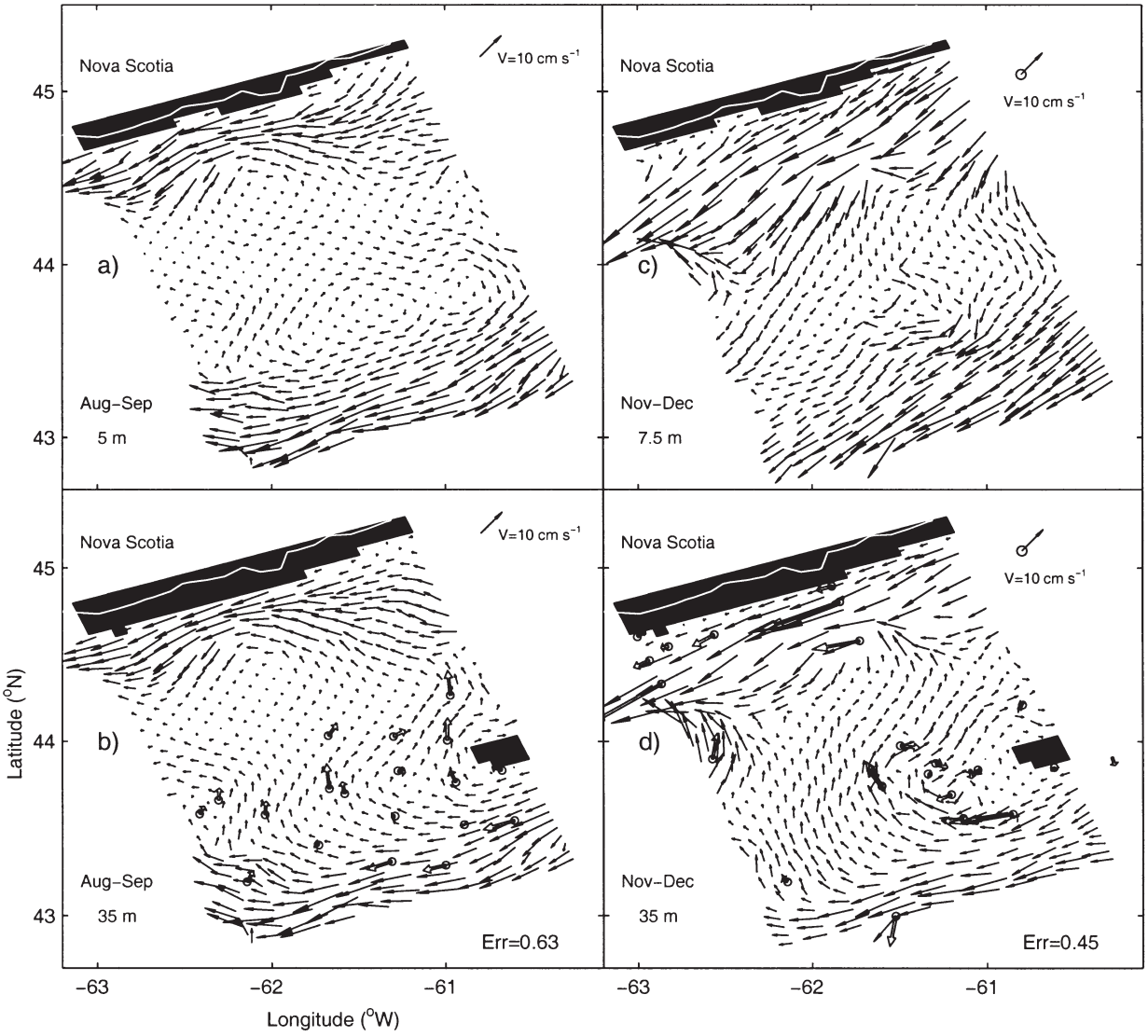

Fig. 10 Horizontal velocities of the optimal state on the 5- and 35-m layers for the summer (a,b) and fall (c,d) respectively.

continue outside our domain and indeed its transport may be greater than we describe, given that we have limited observations off the shelf in deeper water.

Comparisons with observations for the summer and fall seasons are presented in Figs 10 and 11 in which hollow arrows with circles represent measured velocities that were used by the assimilation scheme for the 20–50 m and 50–80 m layers (see Section 3). Hollow arrows without circles mark the velocities that were not assimilated in the model as they were measured either at depths less than 20 m or greater than 80 m or were located outside the computational domain.

1 AUGUST–SEPTEMBER.

The Nova Scotia current flows into our region through the eastern boundary as a broad coastal jet (60–70 km across) with typical velocities of 10 cm s^{-1} (Figs 10a and 10b). It gradually narrows and deflects onshore following the 100-m isobath. Its maximum speed in the upper layer reaches 16 cm s^{-1} near the Halifax line. In the vertical, it spreads up to 100 m near the Liscomb line and up to 130 m when it reaches the Halifax line.

The Emerald Basin region has a weak cyclonic circulation with no current over the centre part of Emerald Basin. The gyre has peak speeds of 2–4 cm s^{-1} near the edges of Emerald Basin with higher velocities in the north, close to the Nova Scotia Current. Unfortunately, we do not have any velocity measurements in that region and so cannot independently confirm these results. The weakness of the absolute velocities in this cyclonic gyre can be explained by opposing the influence of salinity and temperature there, effects that are qualitatively presented in Fig. 4.

The summer circulation over Western and Emerald Banks can be characterized as a relatively strong shelf break jet and a weak north-westward inshore flow. The main part of this north-westward current is concentrated in the current flowing

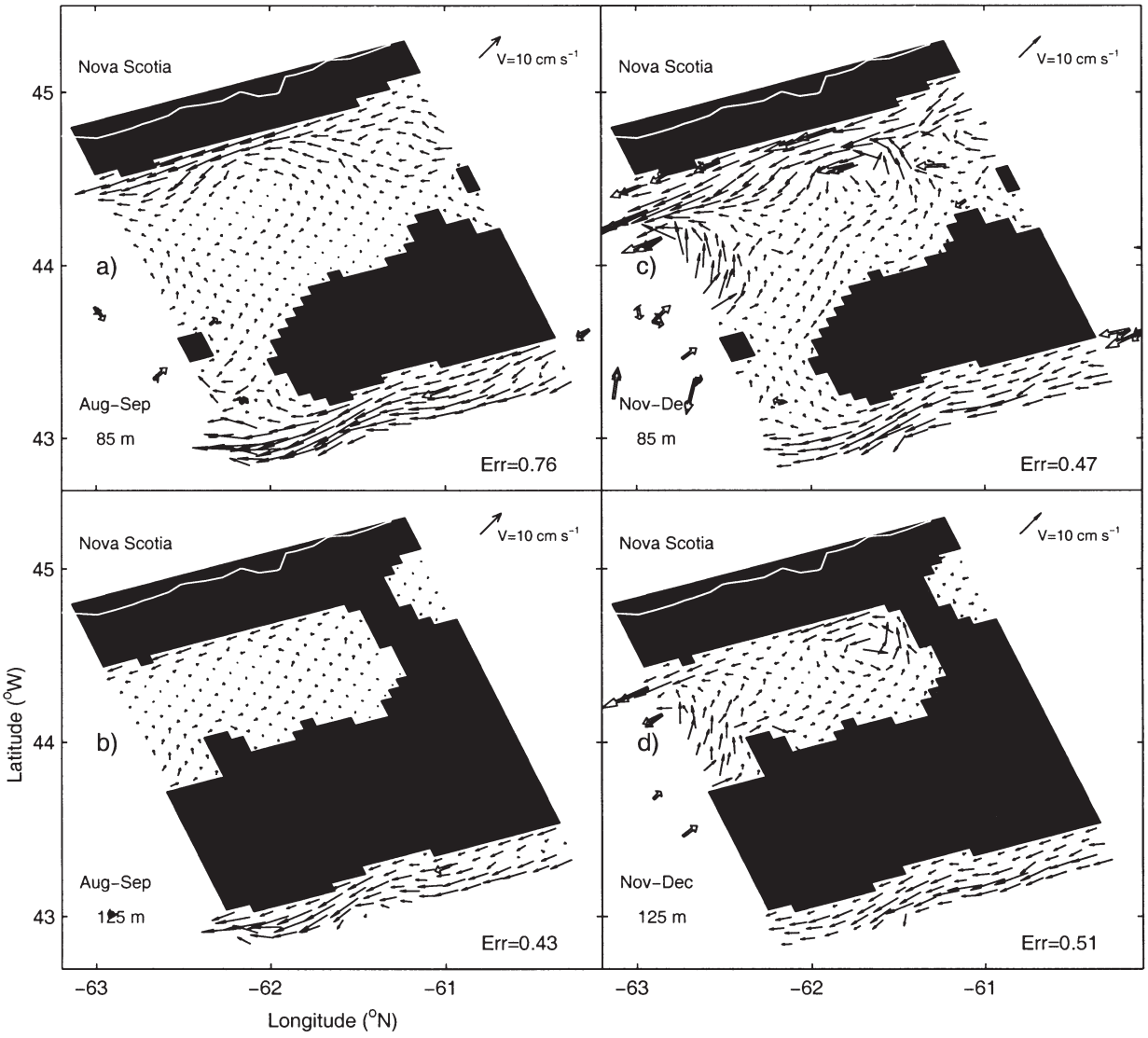

Fig. 11 Horizontal velocities of the optimal state on the 85- and 125-m layers for the summer (a,b) and fall (c,d) respectively.

around the crest of Western Bank with a transport of about 0.05 Sv and typical velocities of 5 cm s^{-1}. This current follows the 70-m isobath around Western Bank and then deflects northward to join the Nova Scotia Current. Another distinct part of inflow from the offshore was found in the subsurface layers in shallow (about 40 m) regions located to the east of the crest of Western Bank (Fig. 10b). However, the depth integrated transport should be negligible because of a southward wind-driven current in the upper layer (Fig. 10a).

Combined with these two parts of north-westward flow concentrated near the Western Bank crest, the channel between Western and Emerald Banks is a third pathway for Atlantic Slope Water (Petrie and Drinkwater, 1993) to cross the shelf break and enter the shelf region. This current, which has a velocity of 5 cm s^{-1} passes through the channel between the two banks and then deflects to the west into Emerald Basin. Some irregularity in this current can be explained by the discrepancy between the real and model topography near the open boundaries. This discrepancy arises due to the necessity of defining some finite difference operators in the variational algorithm and can lead to a mismatch between assimilated real measurements and their model counterparts.

The along-slope current has a velocity of up to 17 cm s^{-1} and shows the influence of topographic steering. The velocities obtained reveal good agreement with observations even in the deep layers (Fig. 11b). Averaged over all the measurements, the discrepancy between observed velocities and their model counterparts is about 50%. According to Fig. 11, the discrepancy between the model and independent observations in the 85- and 125-m levels ranges between 43% and 76%.

Although velocities in the surface (Fig. 10a) and subsurface (Fig. 10b) layers are very similar, differences do exist, which although weak, can play a significant role given that the overall subsurface circulation is weak. For example, in the central part of Emerald Basin the surface circulation has a weak offshore component while the subsurface current is

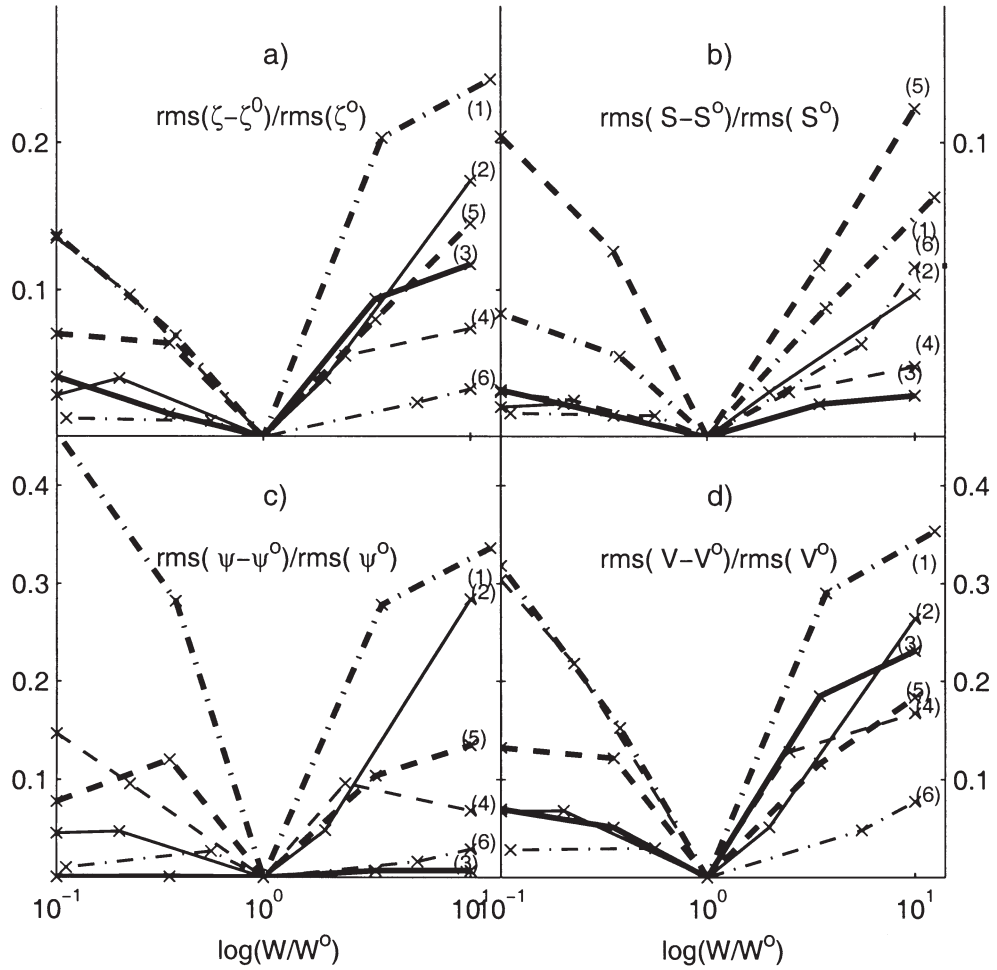

Fig. 12 Dependence of the SSH field (a); salinity field (b); transport function (c) and; velocity field on 25 m on relative changes in the value of covariance functions W_ζ^s - SSH smoothness, curve (1); W_ζ - corresponding to "SSH data" (2); $W\psi$ - smoothness of total transport function (3); W_S^s - temperature and salinity smoothness (4,5); W_S - corresponding to salinity data (6).

onshore. A stronger effect on the eastern side of Western Bank leads to a closing of the anti-cyclonic gyre in the surface layer and velocities of about 4 cm s^{-1}. We speculate that the isolated lens of fresh water on the southern flank of Western and Sable Banks (see Fig. 4a) is formed by the southward surface transports of fresh water out of the Gulf of St. Lawrence. This water flows around Western Bank, mixes with subsurface water and Atlantic surface water and is heated on its way around the bank. The time for circulation around the gyre is about 30 days. If the mean heat flux is about 80 W m^{-2} (Umoh and Thompson, 1994), then we estimate the increase in temperature of a 50-m water column to be about 0.8°C, roughly corresponding to the difference between temperatures in the northern and southern flanks of Western Bank (Fig. 4c). An absence of velocity data in the inner part of the Scotian shelf raises a question about the reliability of our results in this region, however, comparison of our results with the diagnostic circulation as determined by Han et al. (1997) showed very similar transports (0.3 Sv vs. 0.35 Sv in our case) for the Nova Scotia Current in the vicinity of Halifax line. The major differences are the narrowness of the Nova Scotia Current and the weaker absolute velocities of the cyclonic gyre in the Emerald Basin revealed in our calculations. The first is probably a consequence of the initial interpolation of temperature and salinity fields provided before any diagnostic calculations while, in our approach, temperature and salinity can change in our model algorithm. The second may be a result of the absence of observed velocity data in this area.

2 NOVEMBER-DECEMBER

The fall circulation (Figs 10c,d and 11c,d) differs substantially from the summer circulation. The Nova Scotia Current enters the region as a broad (roughly 80 km) jet through the eastern boundary, with speeds up to 20 cm s^{-1} in the upper layer and 4 cm s^{-1} at the 100-m depth. Having entered Emerald Basin, it deflects slightly onshore near the Liscomb line but reaches the same breadth (roughly 80 km) on the Halifax line. Qualitatively this result is in agreement with expected topographic steering in the north-eastern part of our domain (see the topography in Fig. 1a). In the vicinity of the Halifax line surface velocities reach 32 cm s^{-1} and occupy the layer from the surface up to 200 m. As mentioned above, the

transport of the Nova Scotia Current is about 0.9 Sv. In the coastal regions between Liscomb and Halifax, our results show an eastward countercurrent of about 4 cm s^{-1}. Roughly the same current was determined by Han et al. (1997), and described by Andersen and Smith (1989).

The fall circulation in Emerald Basin is defined by an intensified cyclonic circulation with velocities of about 15 cm s^{-1} at the 125-m level and by an inflow current from Western Bank. This current crosses Emerald Basin and joins the Nova Scotia Current between the Halifax and Liscomb lines in the upper layer (Fig. 10d). In the intermediate layer (Fig. 11c) this current forms a cyclonic gyre in Emerald Basin. Strong intensification of the Emerald Basin gyre in the western part of the region is in agreement with observations (Anderson and Smith, 1989) and with the model results of Han et al. (1997). We speculate that intensification of the circulation in the deep layers can lead to significant changes in the water masses' properties (Smith and Schwing, 1991; Fournier et al., 1984).

In the intermediate layers, our calculations revealed a rather narrow (about 15 km) westward current along the north flank of the Western Bank (Fig. 11c) with speeds up to 4 cm s^{-1}. The velocity is close to the direction and absolute value of observations at 100-m depth (Fig. 11c). These data were not used in the assimilation scheme. We believe that this flow could be a continuation of inflow from the channel between Western and Middle Banks. Both the westward current and inflow through the channel can be seen only in the 50–110-m layer. The lower level of the current reaches the maximum depth of the channel. In the surface we obtained eastward currents with 6 cm s^{-1} velocities. As these westward, subsurface currents disturb the local transport function distribution (Fig. 9d) we suggest that they likely influence water formation processes in the eastern part of Emerald Basin.

The across-shelf inflow over Western and Emerald Banks appears as a broad uniform jet with velocities of about 7 cm s^{-1}. The transport of the inflow is approximately 0.1 Sv (Fig. 9d), but only a part of it enters Emerald Basin. The second part feeds the anti-cyclonic current around the crest of Western Bank and around Sable Island. Typical velocities for the along-slope current are up to 24 cm s^{-1}. As in summer, it also follows the topography but has a larger offshore component near the south-western flank of Western Bank (43°N, 61.5°W). Unfortunately, given the limited temperature/salinity data for water deeper than 300 m, there is some uncertainty in the observed differences in seasonal behaviour of the along-slope current. The differences could result from assimilation of velocity observations at this location in fall (Fig. 10d).

The strong north-west winds, which usually start in October, strongly influence the surface layer circulation (Fig. 10c). The comparison between subsurface and surface layers (Figs 10c and 10d) helps to illustrate the wind-driven component of the current which is roughly 3–5 cm s^{-1} south-westward. As in summer, wind effects are most significant on the eastern side of Western Bank. In the fall, these shallow regions are the route for the offshore transport of fresh, cold water (Figs 5a,c).

The mean discrepancy between the observed velocities and their model counterparts for the fall period is roughly 50%. The largest contribution to this figure comes from the errors in the Nova Scotia Current region with extremely high (up to 39 cm s^{-1}) currents (Anderson and Smith, 1989). As seen in Figs 10b,d, in the fall, the distribution of velocity measurements is more uniform over the region and covers both Western Bank and the Nova Scotia Current region. So, despite the fact that the fall demands a more detailed description of the upper boundary layer, we believe that the modelled fall circulation is more reliable than the summer circulation.

5 Sensitivity analysis

Sensitivity analysis is an essential part of any numerical modelling. As described above, the solution of the data assimilation problem depends upon the a priori covariance functions W^{-1}. Being appropriately defined, they permit us to obtain an optimal solution to our problem. Unfortunately, the limited amount of data do not permit unique, accurate estimates of the appropriate covariance function leaving some room for subjectivity in the estimates.

We provide the simplest analysis of departure from the optimal state by exploring the influence of the absolute values of the weight functions W_ζ^s (SSH smoothness), W_ζ (corresponding to the SSH data), W_ψ (smoothness of transport function), W_u (correspondence to the velocity data), (W_θ^s, W_S^s) (smoothness of the temperature and salinity fields), and (W_θ, W_S) (correspondence to the temperature and salinity data). Figures 12a,b,c,d represent the normalized variation of the SSH, transport function and subsurface (25 m) temperature and velocity fields, from its optimal state in relation to changes in the weight functions. The changes in the weight functions are equivalent to a specification of 32% smaller (greater) variance of corresponding physical values; for the smoothing weight functions W_θ^s, W_S^s, the changes are equivalent to an increase (decrease) of the typical spatial scale by about a factor of 2.

The typical changes in SSH were approximately 10% (Fig. 12a). Of course, the SSH was more sensitive to the changes in the weight functions responsible for the SSH smoothing (25%) and the SSH data (18%) as these weight functions have a direct influence on SSH. Changes in the transport and the velocity fields, as fields that are closely connected with SSH, revealed rather similar behaviour (Figs 12c,d). They do show somewhat greater sensitivity (about 30%) to the smoothness W_ζ, consistent with the high level of SSH variance mentioned in Section 2. The strong asymmetry of curve (2) (corresponding to the SSH data) (Figs 12a,c,d) means that the our definition of the W_ζ was close to desirable while artificially simulated SSH (see Section 2) has a minimum effect on our model determination. The symmetry and sharp increase of curve (1) (SSH smoothness) indicates an appropriate and rather narrow range for the selection of the SSH smoothness.

Sensitivity of the salinity field was within 12% of the relative changes for all weight functions (Fig. 12b). The temperature field (not shown) was somewhat more sensitive to the

changes in the weight functions responsible for the SSH data/smoothing and total transport smoothing. Temperature changes may need to be greater than salinity changes to yield the same effect on the SSH and total transport fields, not surprising perhaps given the dominant role of the salinity on the circulation, as discussed above.

In summary, the variational algorithm can be characterized by a weak dependence on most of the weight functions, similar to the work of McIntosh (1990) who studied a simple unconstrained variational problem. The weight functions do have some influence on the calculations but the results are not strongly sensitive to the parameter choices. An obvious advantage of the technique is the ability to provide error estimates for the interpolated fields. A straightforward way to estimate errors is to invert the Hessian matrix $\mathfrak{H}$ associated with the interpolation scheme. In our case it has a dimension of 31,046 $\times$ 31,046 making it difficult to perform the explicit inversion.

For a limited number of observables $\mathfrak{L}_i$, $i = 1,\ldots,N$ it is possible to perform an implicit inversion of $\mathfrak{H}$, i.e., to solve N systems of equations $\mathfrak{H}X = \mathfrak{L}_i$, each requiring approximately the same amount of computation as one assimilation run. To obtain, for example, the 3D salinity error distribution in this manner, one would have to solve 12113 (the number of salinity points) systems of equations an equivalent number of times, which lies beyond our present computational capacity.

6 Discussion and conclusions

In this study, we reconstructed the mean quasi-stationary circulation for the summer and fall on the outer part of the Scotian Shelf taking into account all available data for this region. The data consisted of direct atmospheric and oceanic measurements (temperature, salinity, velocity and wind stress) and indirect climate estimates for the surface heat and salt fluxes. The variational approach combined with the fine resolution grid allowed us to clarify some details of the mean circulation for the outer Scotian Shelf, and in particular for Western Bank (Han et al., 1997). The analysis also revealed several new features of the circulation for the August–September and November–December periods.

We applied a rather simplified model but, noting the conclusion of Han et al. (1997) that baroclinic processes dominate the circulation in the Western Bank region, we believe that our results are quite realistic. Even in the regions with limited data (in particular the north-eastern part of our region), we determined a circulation field that at least has the same basic characteristics as found by Han et al. (1997). Our sensitivity analysis and the fast convergence of the major integral transport features to their optimal values confirms the validity of our results.

The main advantage of our approach is the independence of the open boundary conditions that have to be specified in the classical diagnostic calculation and introduce subjectivity in the final circulation pattern. Our transport constraints have a soft or "weak" character and are based on realistic estimates and real data. We minimized smoothing by using the model equations as an interpolation algorithm. Although there may be some errors in the estimates of the covariance function, their influence is minimized since the state variables are constrained by the model equations. The sensitivity analysis presented above supports this interpretation.

Unfortunately the limited extent of our spatial domain does not allow better resolution of the influence of wind forcing. We note that an accurate description of the upper layer in the shallow regions requires complicated turbulent models (for example Mellor and Yamada, 1982), which are not included in our algorithm. Nonetheless the detailed features of our results are in agreement with the observed circulation even in the upper layer.

The main results of our study are: (1) The seasonal changes from summer to fall cause an intensification of and spatial changes in the circulation pattern around Western Bank. The intensification of the circulation covers all of our model domain on the central Scotian Shelf. The fall intensification is stronger in the deeper layers than in the surface. (2) During summer, the inflow of the Atlantic surface water into the inner part of the Scotian Shelf is relatively weak and is concentrated in the eastern part of Emerald Basin. In fall, the inflow occurs primarily in the central part of Emerald Basin. (3) The countercurrent in the 60–120-m layer on the northern flank of the Western Bank can cause significant changes in transport and as a consequence can influence water mass formation. (4) The influence of the wind on the circulation in the upper layer is crucial both in the summer and in the fall. Its influence in the shallow regions produces offshore transport in the surface layer which explains the appearance of fresh water in the eastern part of our domain. (5) The current in the channel between Western and Middle Banks has an eastward direction in the surface layer but is directed westward in the bottom layer.

Acknowledgements

This study was made possible by support to the GLOBEC Canada program from the Natural Sciences and Engineering Research Council to BdeY, and by the Frontier Research System for Global Change to MY. We gratefully acknowledge their support. We also thank our colleagues in the Western Bank program, in particular Drs. C. Reiss and C. Taggart. We thank two reviewers for detailed and helpful comments.

References

ANDERSON, C. and P.C. SMITH. 1989. Oceanographic observation on the Scotian Shelf during CASP. ATMOSPHERE-OCEAN, **27**: 130–156.

BRANDER, K. and P. HURLEY. 1992. Distribution of early stage Atlantic cod (*Gadus morhua*), haddock (*Melanogrammus aeglifinus*), and witch flounder (*Glyptocephalus synogiossus*) eggs on the Scotian Shelf: A reappraisal of evidence on the coupling of cod spawning and plankton production. *Can. J. Fish. Aquat. Sci.* **49**: 238–251.

BRETHERTON, F.P.; R.E. DAVIS and C.B. FANDRY. 1976. A technique for objective analysis and design of oceanographic experiments applied to MODE-73. *Deep Sea Res.* **23**: 559–582.

CSANADY, G.T. and P. HAMILTON. 1988. Circulation of slope water. *Cont. Shelf Res.* **8**: 565–624.

DA SILVA, A.; A.C. YOUNG and S. LEVITUS. 1994. Atlas of Surface Marine Data 1994, Volume 1: Algorithms and Procedures. NOAA Atlas NESDIS 6, U.S. Department of Commerce, Washington, D.C. 83 pp.

FOURNIER, R.O.; M. VAN DET, N.B. NARGREAVES, J.S. WILSON, T.A. CLAIR and R. ERNST. 1984. Physical factors controlling summer distribution of chlorophyll off southwestern Nova Scotia. *Limnol. Oceanogr*. **29**: 517–526.

GANDIN, L. 1963. Objective Analysis of Meteorological Fields. (Leningrad: Grindromet). English translation (Jerusalem: Israel Program for Scientific Translation). 1965, 266 pp.

GILBERT, J.C. and C. LEMARECHAL. 1989. Some numerical experiments with variable storage quasi-Newton algorithms. *Math. Program*. **45**: 407–455.

GILL, A.E. 1982. *Atmosphere Ocean Dynamics*. Academic Press, New York, 662 pp.

GREENBERG, D.A.; J.W. LODER, Y. SHEN, D.R. LYNCH and C.E. NAIMIE. 1997. Spatial and temporal structure of the barotropic response of the Scotian Shelf and Gulf of Maine to surface and wind stress: A model based study. *J. Geophys. Res.* **102**: 20,897–20,916.

GRIFFIN, D.A. and K.R. THOMPSON. 1996. The adjoint method of data assimilation used operationally for shelf circulation. *J. Geophys. Res.* **101**: 3457–3477.

GROTOV, A.S.; D.A. NECHAEV, G.G. PANTELEEV and M.I. YAREMCHUK. 1998. Large scale circulation in the Bellingshausen and Amundsen seas as a variational inverse of climatological data. *J. Geophys. Res.* **103**: 13011–13022.

HAN, G.; C.G. HANNAH, J.W. LODER and P.C. SMITH. 1997. Seasonal variation of the three-dimensional mean circulation over the Scotian Shelf. *J. Geophys. Res.* **102**: 1011–1025.

HOUGHTON, R.W.; P.C. SMITH and R.O. FOURNIER. 1978. A simple box model for cross-shelf mixing on the Scotian Shelf. *J. Fish. Res. Board Can.* **35**: 414–421.

ISHIZAK, J.H. 1994. A simulation of the abyssal circulation in the North Pacific ocean. *J. Phys. Oceanogr*. **24**: p.1941–1954.

ISEMER, H.J. and L. HASSE. 1987. *The Bunker Climate Atlas of the North Atlantic Ocean*, Vol. 2: *Air-Sea Interactions*, Springer-Verlag, New York. 225 pp.

LARGE, W.G. and S. POND 1982. Sensible and Latent Heat Flux measurements over the Ocean. *J. Phys. Oceanogr*. **12**: 464–482.

LODER, J.W.; G. HAN, C.G. HANNAH, D.A. GREENBERG and P.C. SMITH. 1997. Hydrography and baroclinic circulation in the Scotian Shelf region: Winter vs. summer. *Can. J. Fish. Aquat. Sci.* **54**: (suppl .1) 40–56.

MCINTOSH, P.C. 1990. Oceanographic data interpolation: objective analysis and splines. *J. Geophys. Res.* **35**: 13529–13541.

MCLELLAN, H.J. 1954. Temperature-salinity relations and mixing on the Scotian Shelf. *J. Fish. Res. Board Can.* **11**: 419–430.

———; L.M. LAUZIER and W.B. BAILEY. 1953. The slope water off the Scotian Shelf. *J. Fish. Res. Board Can.* **10**: 155–176.

MELLOR, G.L. and T. YAMADA. 1982. Development of a turbulence close model for geophysical fluid problems. *Rev. Geophys. Space Phys.* **20**: 851–875.

NECHAEV, D.A.; G.G. PANTELEEV and M.I. YAREMCHUCK. 1997. Circulation in the Amundsen and Bellingshausen seas derived from atmospheric and oceanic climatologies. *Okeanologia*, **37(5)**: 586–594.

PETRIE, B. and P.C. SMITH. 1977. Low-frequency motion on the Scotian Shelf and Slope. *Atmosphere*, **15**: 117–140.

——— and K. DRINKWATER. 1993. Temperature and salinity variability on the Scotian Shelf and in the Gulf of Maine 1945–1990. *J. Geophys. Res.* **98**: 20,079–20,089.

REISS, C.; G. PANTELEEV, C.T. TAGGART, J. SHENG and B. DEYOUNG. 2000. Density driven circulation on the Scotian Shelf: Implications for larval fish retention, transport and survival. *Fish. Oceanogr*. **9**: 195–213.

SANDERSON, B. 1995. Structure of an eddy measured with drifters. *J. Geophys. Res.* **100**: 6761–6776.

SHENG, J. and K.R. THOMPSON. 1996. A robust method for diagnosing regional shelf circulation from scattered density profiles. *J. Geophys. Res.* **101**: 25647–25659.

SMITH, P.C. and B.D. PETRIE. 1982. Low-frequency circulation at the edge of Scotian Shelf. *J. Phys. Ocean.* **12**: 28–55.

——— and F.B. SCHWING. 1991. Mean circulation and variability on the eastern Canadian continental shelf. *Cont. Shelf Res.* **11**: 977–1012.

TAGGART, C.T.; K.R. THOMPSON, G.R. MAILLET, S.R. LOCHMANN and D.E. GRIFFIN. 1996. Abundance and distribution of larval cod (*Gadus morhua*) and zooplankton in a gyre-like water mass on the Scotian Shelf. *In*: Proc. Intl. Workshop on Survival Strategies in Early Life Stages of Marine Resources. Y.Y. Watanabe and Y. Oozecki (Eds) Rotterdam Holland, 1994. A.A. Balkema Publishers, pp. 155–173.

THACKER, W.C. 1989. On the role of the Hessian matrix in fitting models to measurements. *J. Geophys. Res.* **94**: 6177–6196.

THOMPSON, K.R. and D.A. GRIFFIN. 1998. A model of the circulation on the outer Scotian Shelf with open boundary conditions inferred by data assimilation. *J. Geophys. Res.* **103**: 30,641–30,660.

UMOH, J. and K.R. THOMPSON. 1994. Surface heat flux, horizontal advection and the seasonal evolution of water temperature on the Scotian Shelf. *J. Geophys. Res.* **99**: 20,403–20,416.

UNESCO. 1981. Tenth report of the joint panel on oceanographic tables and standards. UNESCO Tech. Papers in Mar. Sci., No. 36, 25 pp.

WUNSCH, C. 1994. Dynamically consistent hydrography and absolute velocity in the eastern North Atlantic Ocean. *J. Geophys. Res.* **99**: 14071–14090.